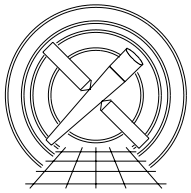

MIT Kavli Institute **Chandra X-Ray Center**

MEMORANDUM
September 21, 2010

To:	File
From:	David P. Huenemoerder, SDS
Subject:	Notes on sub-pixel event algorithm effect for *Chandra* grating spectra.
Revision:	1.0
URL:	`http://space.mit.edu/cxc/docs/subpix_tg.pdf`
File:	`/nfs/cxc/h3/dph/CXC/Subpix_dev/Doc/subpix_tg.pdf`

1 About EDSER

The Energy Dependent Subpixel Event Repositioning (EDSER) algorithm of Li et al (2004 ApJ 610, 1204; <http://adsabs.harvard.edu/abs/2004ApJ...610.1204L>) has been implemented in `acis_process_events` in the development version of CIAO. The algorithm provides significant improvement in the point-spread-function (PSF) for the Back-Illuminated (BI) CCDs, and some for Front-Illuminated CCDs (FI). (For reference, Figures 1 and 8 from Li et al (2004) have been reproduced in Appendix A.)

Before we decide to also implement the algorithm in `tg_resolve_events`, we should assess its effect on grating spectra.

2 Processing

The `acis_process_events` algorithm applies the subpixel algorithm on chip coordinates and writes corrected sky coordinates. To examine the effect on grating spectra, we need to perform custom extraction since `tg_resolve_events` does not use the sky coordinates but derives grating coordinates from chip coordinates. The custom processing takes the EDSER event file from `acis_process_events` (without pixel randomization) and applies `tg_resolve_events` to produce grating coordinates for each event (specifically, `tg_m`, `tg_part`, `tg_lam`). Since the events in the input and output files correspond, we use the file with grating coordinates to define an event filter based on their grating, order, and wavelengths (and also select standard grades and good status), then select those events from both the EDSER file and standard files. The events are then rotated according to the spacecraft roll (from the event file's header) and grating clocking angle (available from the CALDB "`geom[gratings]`" file) in dispersion and cross-dispersion coordinates parallel to x and y axes, respectively. The events are binned in dispersion and cross-dispersion directions, and a wavelength scale is derived by fitting the `tg_lam` values vs the rotated coordinate along the dispersion. Count profiles were fit for several lines, from both BI and FI CCDs, and from HEG and MEG arms, using ISIS and a model comprised of a Lorentzian plus a polynomial continuum (no responses were used). The fits provide the line center, full-width half-maximum (FWHM), and area. Confidence limits were also computed for the Lorentzian parameters. We have looked at results for strong coronal emission line sources and two X-ray binary sources with strong Fe K emission (see Table 1).

Table 1: Observation Info

obsid	Name	$T_{\rm exp}$ [ks]	Rate [counts/s]	$f_{\rm x}(1.5-25\,\text{Å})$ $[10^{-12}\ \text{ergs}\,\text{cm}^{-2}\,\text{s}^{-1}]$
10599	Capella	29	2.4	120
15	TZ CrB	84	1.8	75
6132	CC Eri	30	1.3	64
6282	σ Gem	58	2.8	120
1927	Vela X-1	29	6.6	2700
3433	GX 301-2	59	3.7	2400

3 Diagnostics

3.1 Event Distributions

From visual inspection of the event distribution histograms, we can see that the BI profiles are improved in shorter wavelength regions. Figures 1–5 show the event distributions and histograms for a few lines, CCDs, and grating types for ObsID 6282. Each group of three panels shows the event locations in wavelength and cross-dispersion coordinates (lower left), the dispersion histogram (above) and cross-dispersion histogram (to the right). Red signifies the standard processing, and blue the EDSER results. The grating arm, order, and CCD type are given in the title of the upper panel.

The cross-dispersion profiles have higher signal because they include events from a relatively wide spectral region, of about 1 Å.

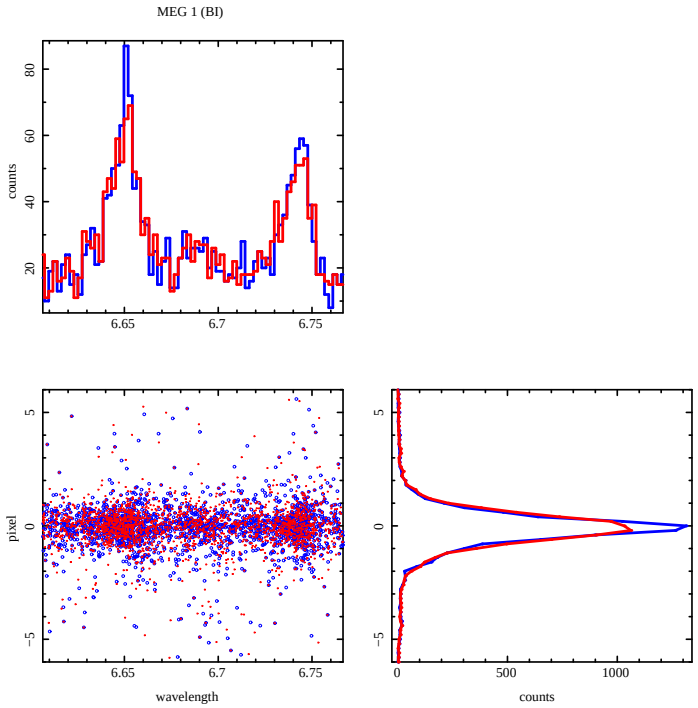

Figure 1: Event distributions from ObsID 6282, σ Gem, a coronally active star. In the set of 3 panels, the lower left box shows the event coordinates, above which is the along-dispersion histogram, and to the right, the cross-dispersion histogram. This shows the Si XIII region for MEG positive first order which is on a BI CCD.

In Figure 1, it is clear that both the in-dispersion and cross-dispersion profiles in the Si XIII region are more peaked with EDSER processing (blue) than standard (red) for the BI CCD. Figure 2 shows the same region for the MEG negative first order, from an FI CCD. As expected (based on Li et al (2004) plots; see Appendix A) the distributions show no improvement with EDSER.

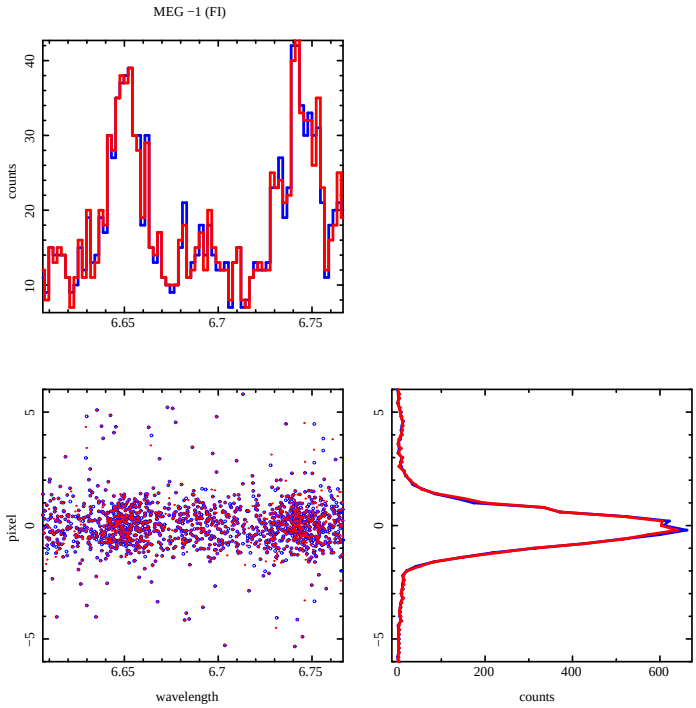

Figure 2: Similar to previous figure, but for the FI CCD.

Figure 3 shows similar behavior in the Mg XII region.

At longer wavelengths, the cross-dispersion astigmatic profile and other grating aberrations (such as period errors) become more significant. This additional spread appears to dominate any gain from EDSER, even on the BI CCDs. Figure 4 shows the profiles for the O VIII line at 18.97 Å.

Figure 5 shows the high-signal Ne X region from an FI CCD. EDSER and standard processing give nearly indistinguishable results.

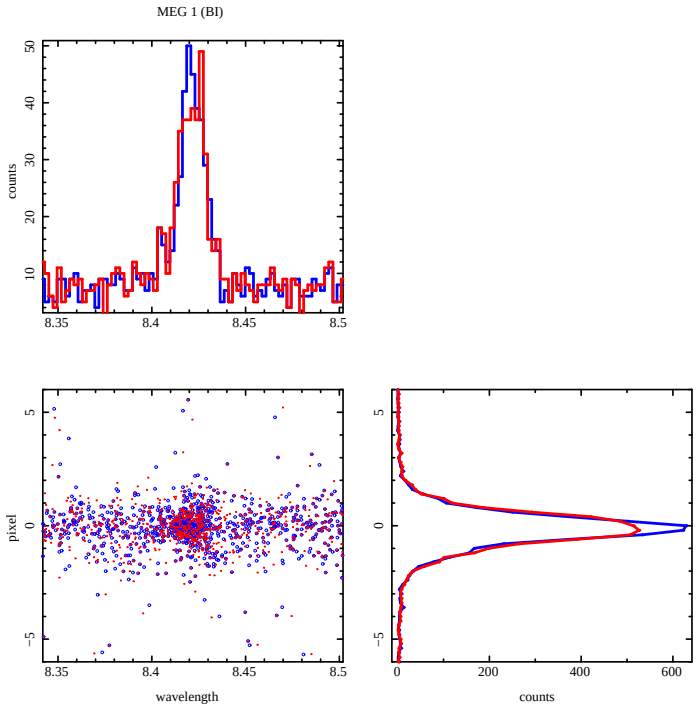

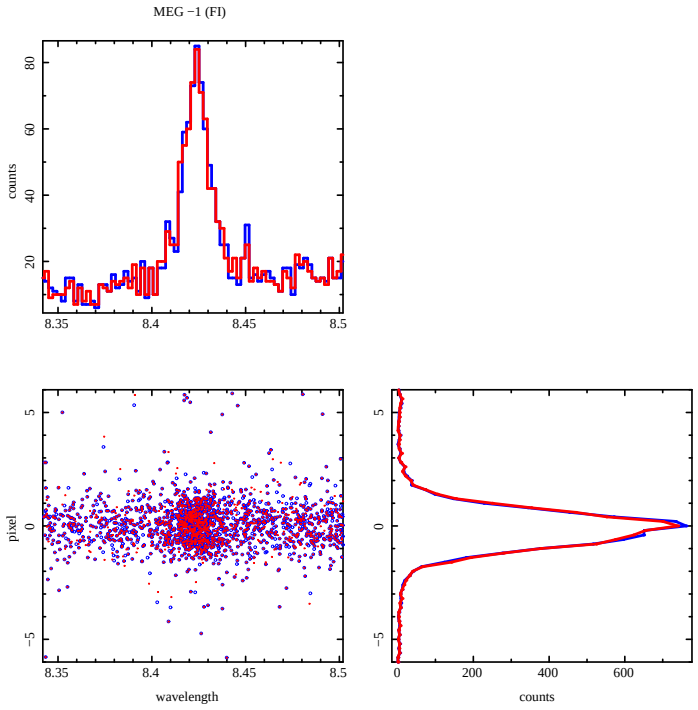

Figure 3: Event distributions for Mg XII H-Lyα as detected by a BI CCD (top), or FI (bottom).

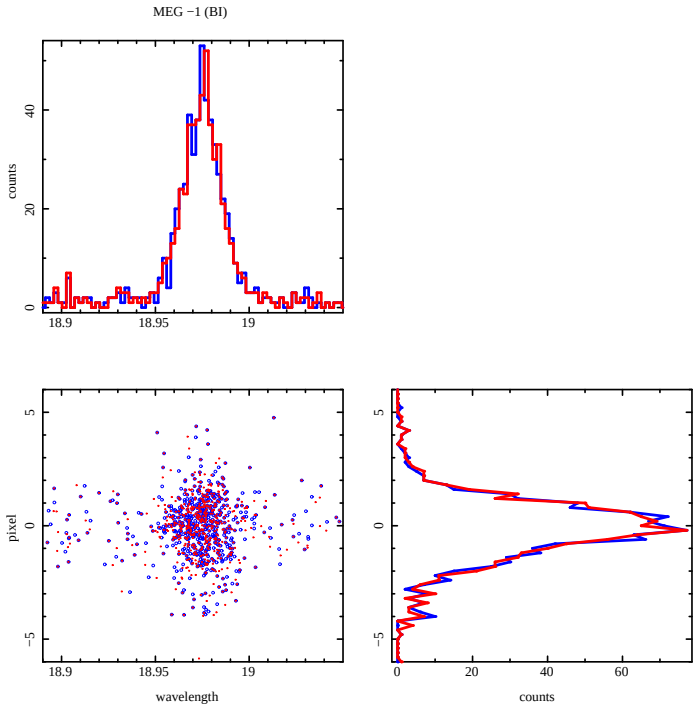

Figure 4: The effect is absent at longer wavelengths where the grating aberrations enlarge the profile. O VIII H-Lyα on a BI CCD, which shows no obvious gain with EDSER.

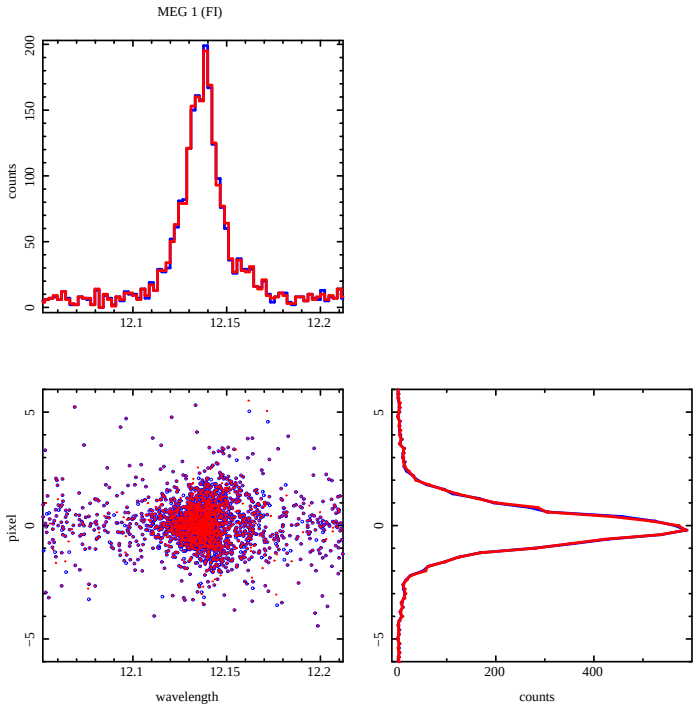

Figure 5: Ne X H-Lyα on an FI CCD: no effect seen even at very high signal to noise.

We contrast this with an example of a strong Fe K line source (GX 301-2, obsid 3433; Figure 6) for which we have both BI and FI profiles at a relatively small diffraction angle, where we might expect the spatial PSF to dominate. We see improvement clearly in the cross-dispersion profiles for both BI and FI as well as in HEG and MEG. Presumably, the effect is also present in the dispersion profile, but somewhat harder to discern due to the lower signal-to-noise ratio.

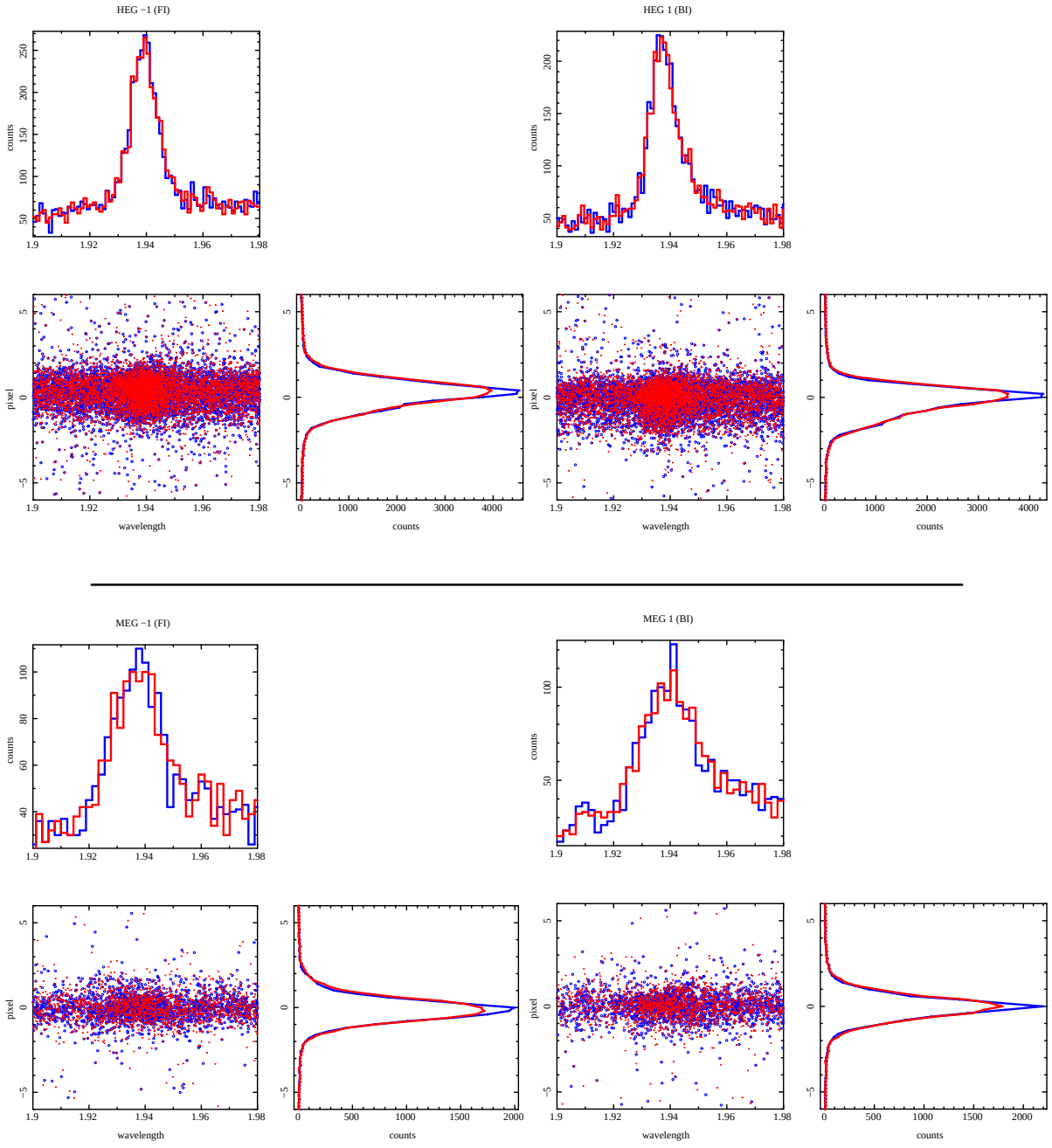

Figure 6: Fe K for HEG (top) and MEG (bottom).

3.2 Line Profile Fitting

For BI CCDs at the shorter wavelengths, we expect some improvement in the line spread function and hence we might expect some improvement in the confidence limits on the line centroid (the centroid as well as the flux should not change under EDSER processing). The following plots show the mean centroid and confidence intervals. In all plots, the large red circles are for features on BI CCDs, and small black circles are from FI CCDs. Confidence is given at 90% limits.

Figure 7 upper left shows the centroid residuals against the theoretical wavelenths. The mean could be non-zero due to effects of blends and line-of-sight velocity. The top right shows the same residuals in velocity units. The lower panel shows the residuals between EDSER and standard proccessed data's velocities (rather than the theoretical line wavelengths). This is, as expected, zero within the uncertainties.

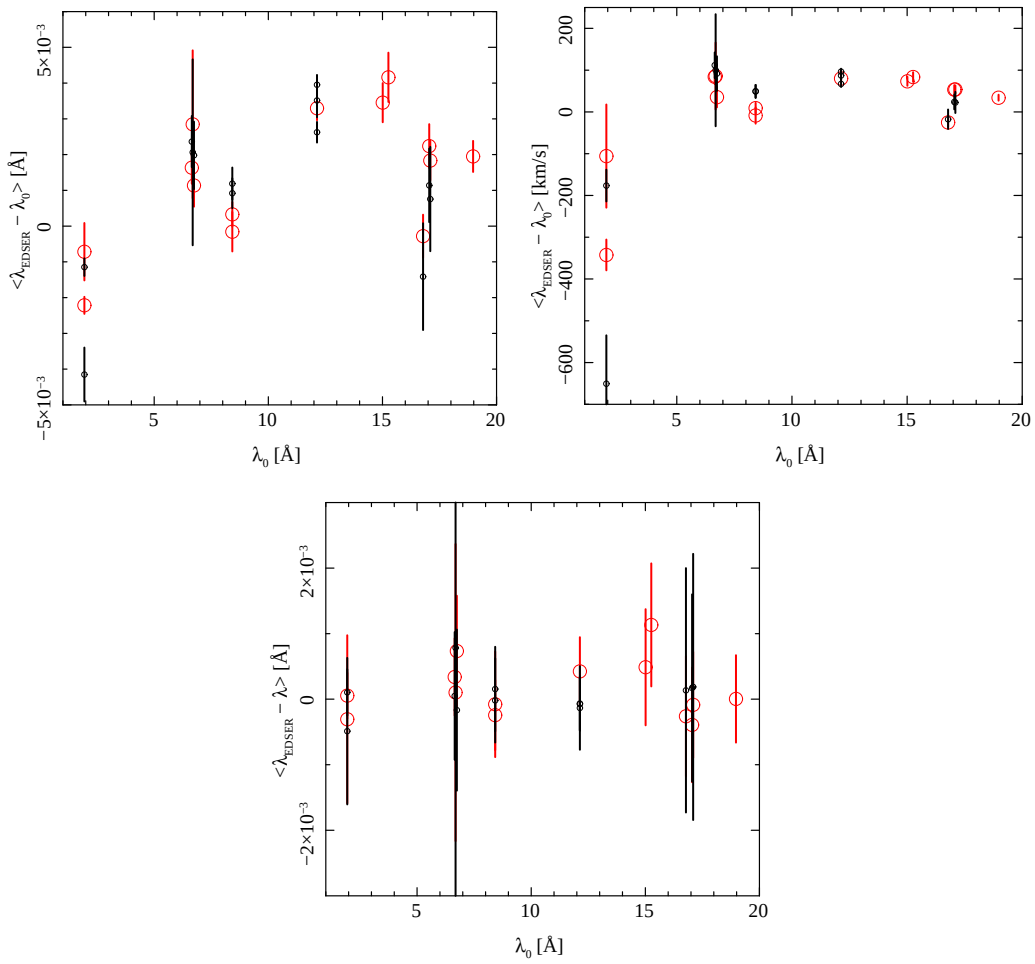

Figure 7: Top: Mean centroid residuals of the EDSER centers (λ_{EDSER}) to the theoretical wavelengths (λ_0). Bottom: the EDSER center residuals relative to those of standard processing. Large red circles denote features from a BI CCD, while small black circles are from an FI CCD. Error bars represent 90% confidence. Values have been averaged over the observations.

Figure 8 shows the difference between the EDSER line center confidence limits and those from standard processing. Here, a more negative number means that the confidence limits are smaller — the line centroid is better determined. (Left is in wavelength units, right in velocity). While the mean of the red (BI) measurements is negative, it is not strongly different from the FI values.

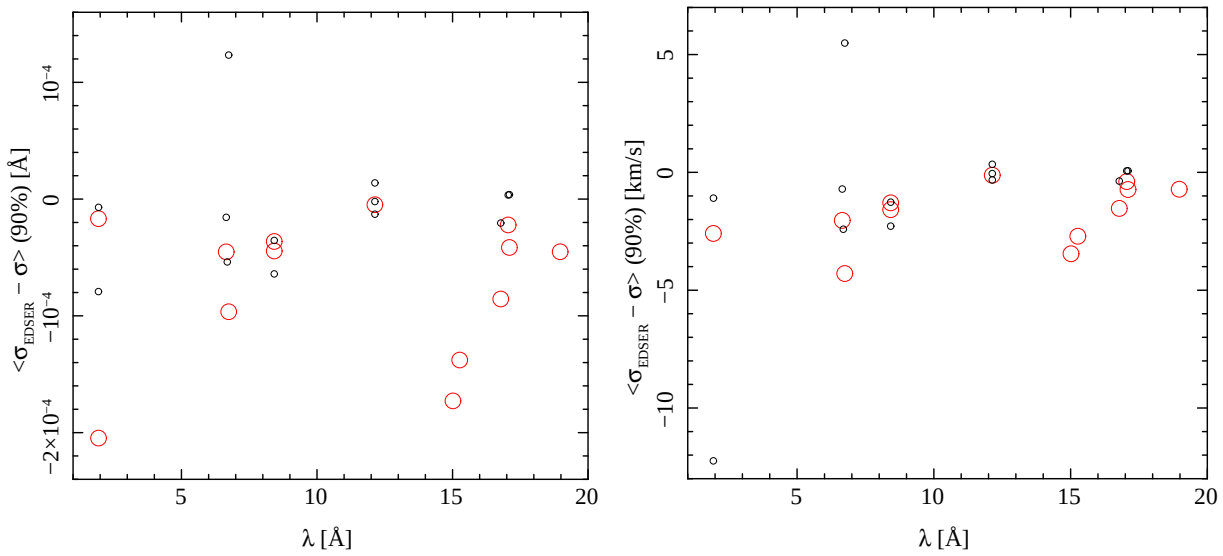

Figure 8: Residuals in the line center 90% confidence limits between EDSER and standard processing, plotted against the standard processing line centers. Large red circles denote features from a BI CCD, while small black circles are from an FI CCD.

Figure 9 shows the same residuals as a fraction of the standard processing results. We see that we can expect about a 10% improvement in the line center determination on the BI CCDs.

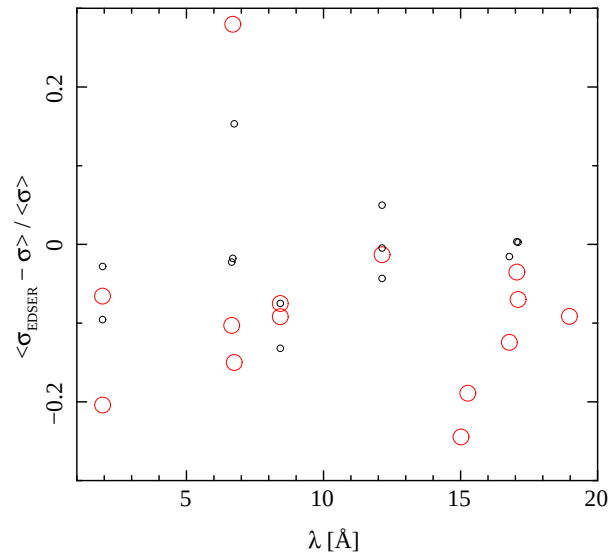

Figure 9: Fractional change in the line-center confidence limits. A negative number means a smaller confidence interval.

4 LETG Considerations

While tests were only done for HETG/ACIS data, there is no reason to expect a larger effect for LETG/ACIS. The ACIS effects of EDSER would be of the same spatial scale. However, there are additional competing terms in the LETG PSF, the coarse and fine supports' cross-dispersion. These additional blur terms would conspire to reduce any gain from the sub-pixel correction algorithms and make it even less significant than for HETG.

5 Conclusions

Advantages: There is detectable, but small improvement in the line centroid confidence limits using EDSER, mostly for BI CCDs, yielding about a 10–20% improvement in the accuracy of the line position.

Disadvantages: with EDSER, the line profile is currently uncalibrated. There is no corresponding grating RMF, so neither the line-spread-function or cross-dispersion enclosed-energy-fraction will be accurate.

There is no compelling reason to include an option to run EDSER in `tg_resolve_events`.

A Figures from Li e al. (2004)

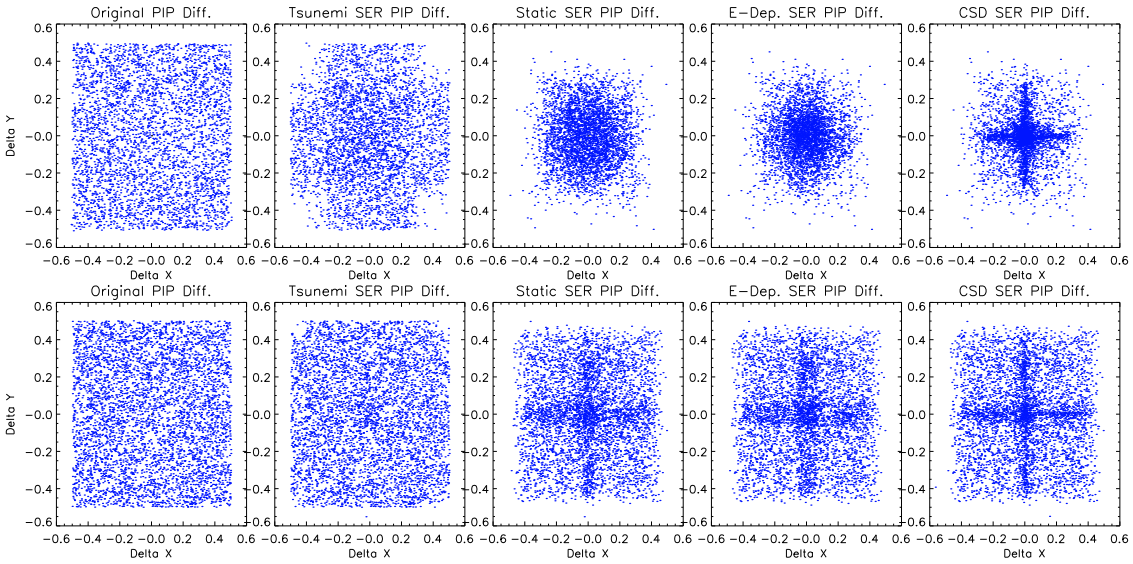

Figure 10: Li et al 2004 Figure 2; Top: BI; bottom: FI. The "EDSER" algorithm implemented in `acis_process_events` is the 4th box from the left.

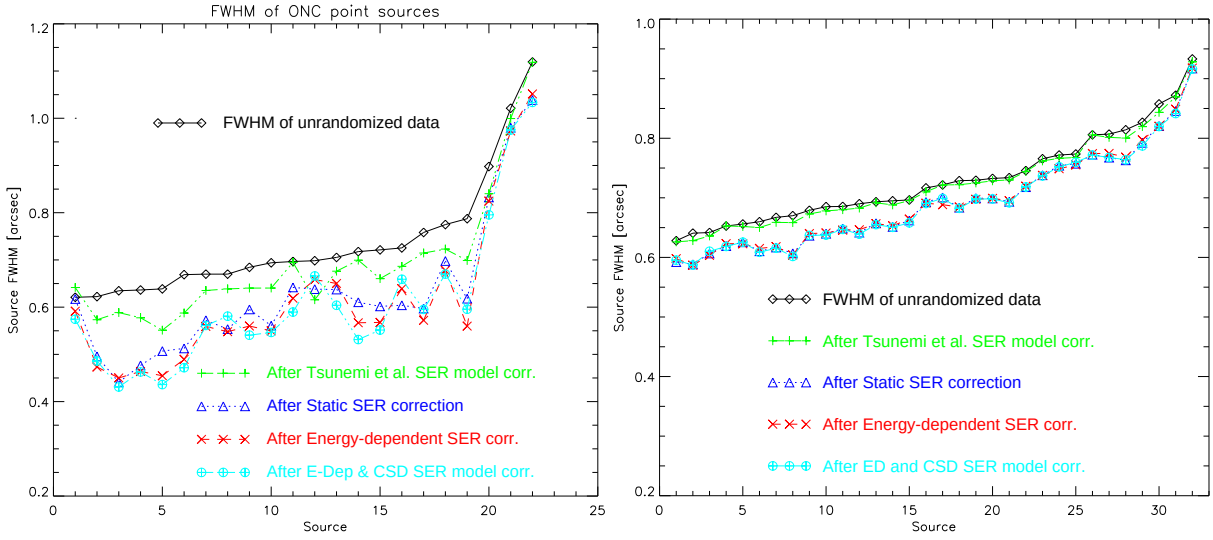

Figure 11: Li et al 2004 Figure 8; Left: BI; right: FI. EDSER is shown by the red curve with "X" symbols